A PASSIVELY TEMPERATURE-COMPENSATED DUAL-FREQUENCY ALN-ON-SILICON RESONATOR FOR ACCURATE PRESSURE SENSING

Qingyun Xie, Nan Wang, Chengliang Sun, Andrew B. Randles, Pushpapraj Singh, Xiaolin Zhang, and Yuandong Gu

Institute of Microelectronics, A*STAR (Agency for Science, Technology and Research), SINGAPORE

ABSTRACT

This paper reports a passively temperature-compensated dual-frequency micromachined resonator which has been experimentally demonstrated to perform accurate sensing of differential pressure. This resonating device incorporates passive temperature compensation techniques, different sub-resonator cavity structures and dual-resonance frequency property, all aimed at applying it in accurate pressure sensing. Its application as an acoustic wave pressure sensor has been demonstrated, with low non-linearity of 1.20 % F.S. over a pressure range of 150 psi, and low thermal zero shift of 0.15 % F.S./°C over a temperature range of 360 °C. The reported device has promising potential for accurate wide-range pressure sensing over wide temperature range, yet minimally affected by ambient temperature, in ruggedized environments like oil-drilling.

INTRODUCTION

Pressure sensors are employed in areas of harsh environments, e.g. aeronautic and oil-drilling industry. [1] The sensing of differential pressure using acoustic wave resonant methods is inevitably affected by ambient temperature, especially if the temperature fluctuates significantly. On the other hand, to enhance the temperature stability of resonance behavior, MEMS resonators feature various active and passive temperature-compensation techniques, of which the latter has merits like lower power consumption than the active schemes. [2, 3] Efforts are made to create CMOS-compatible pressure sensors suitable for high temperature ruggedized environments. However, the thermal shift problem remains pertinent in wide-temperature range pressure sensing, but has not been sufficiently addressed. [4] This gives rise to the need to introduce temperature compensation in these pressure sensors.

DESIGN AND FABRICATION

An aluminum nitride (AlN)-on-silicon (Si) resonator is designed. This resonator is capable of supporting quasi-surface acoustic wave (SAW) modes on the composite plate made of AlN, polycrystalline silicon (poly-Si), and silicon dioxide (SiO_2). Fig. 1(a) and 1(b) presents the design of two types of devices designed. In order to enhance the temperature stability of the devices, an oxide trench array (OTA) was added to the poly-Si layer as a passive temperature compensation structure. The OTA is absent in the reference design to evaluate the effectiveness of OTA in temperature compensation. The resonator is excited by an inter-digitatated transducer (IDT) made of molybdenum and situated on top of the resonator structure.

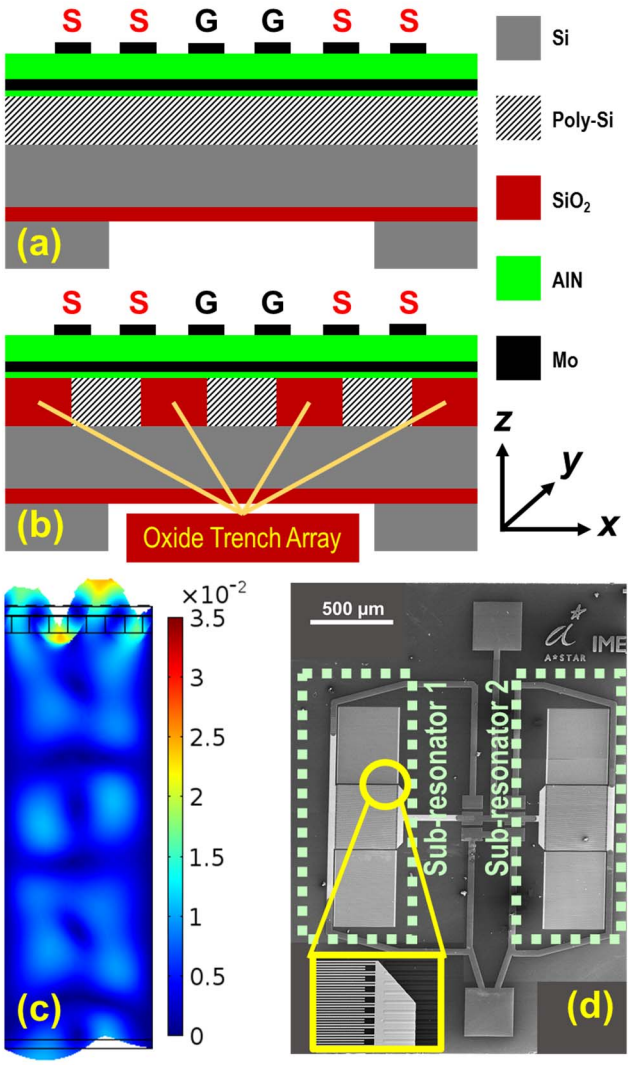

Figure 1: Dual-frequency resonating device featuring proposed temperature compensation technique.
(a) Cross-section of a sub-resonator without OTA.
(b) Cross-section of a sub-resonator with OTA.
(c) Simulation of the quasi-SAW mode shape supported by the resonator structure with OTA. The scale bar to the right represents mechanical displacement in units of μm.
(d) Scanning electron microscope image of dual-frequency resonating device. Close-up views of the oxide trench array are presented in the insets. Sub-resonator 1 generates mode 1, and backside circular cavity is present. Sub-resonator 2 generates mode 2, and is not backside etched.

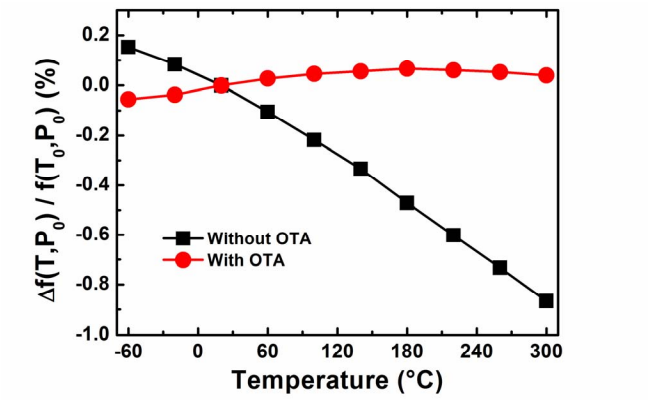

Figure 2: Resonance frequency shift for devices with and without oxide trench array as a passive temperature compensation structure. Here, $T_0 = T_{rm}$.

Finite element simulations were conducted using COMSOL Multiphysics to investigate the resonance modes of the resonating design. The simulation mode shape as illustrated in Fig. 1(c) verifies that, this resonating device design with OTA supports the quasi-SAW mode.

It is a well-known theory for elastic waves traveling in solids, that, to the first order, the resonance frequency f of any acoustic wave mode is given by $f \approx \frac{1}{\lambda}\sqrt{\frac{E}{\rho}}$, where λ is the periodicity of the inter-digital electrodes, E is the effective Young's modulus, and ρ is the effective density of the resonating material. [5] In the case of this reported device, all three of the above variables are functions of differential pressure (between the top and bottom surfaces of the membrane) and/or temperature. Hence, the device performance under temperature and pressure could be characterized, by extracting the resonance frequency at each temperature and pressure.

Both designs, namely the devices with and the reference counterparts without OTA, were fabricated on the same wafer, based on our in-house AlN-on-Si platform. The process flow is designed to be CMOS-compatible. 8-inch silicon-on-insulator (SOI) wafers, with a device layer of 50 µm and a buried oxide (BOX) layer of 1 µm, are used. Firstly, a layer of thermal oxide of thickness 2 µm is grown and patterned. All regions other than the OTA regions are etched. The etched cavities are filled with polycrystalline silicon (poly-Si). Chemical-mechanical polishing (CMP) is performed to ensure a uniform thickness of OTA and poly-Si. Next, layers of AlN (seed layer), bottom Mo, AlN and top Mo of thicknesses 20 nm, 0.2 µm, and 1.2 µm and 0.2 µm respectively, are deposited successively. In order to obtain the IDTs, the top Mo is patterned. Lastly, a backside etch is performed to release the structure. An image of the fabricated devices, taken using a scanning electron microscope (SEM), is presented in Fig. 1(d).

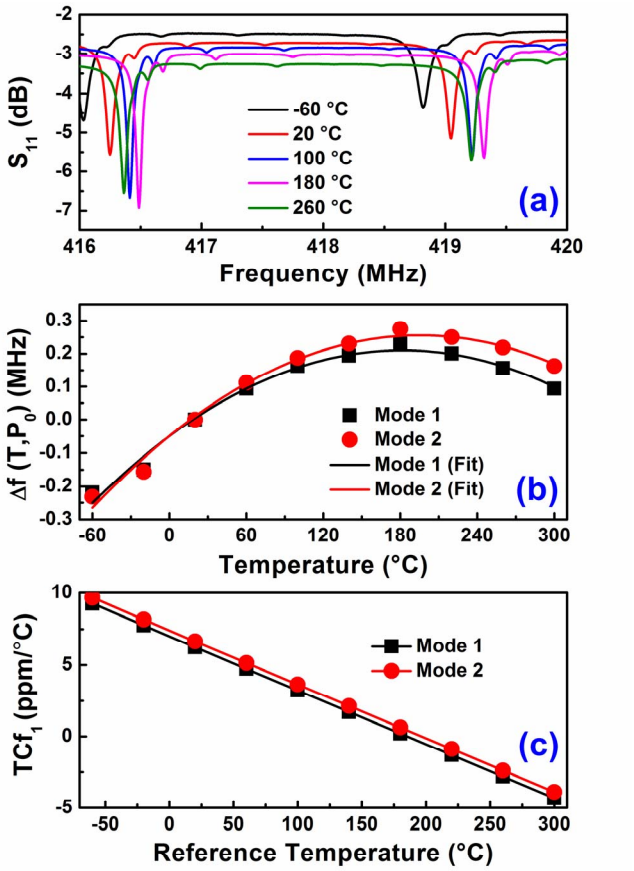

Figure 3: Temperature response of dual-frequency resonating device.
(a) S_{11} response for various temperatures.
(b) Shifts in the two resonance frequencies of the dual-frequency resonating device as a function of temperature.
(c) Variation of TCf_1 as a function of reference temperature T_0, for the two resonance frequencies.

DEVICE CHARACTERIZATION

Temperature Effects

The resonance frequency $f(T, P_0)$ may be described as a function of temperature T at constant pressure P_0, by the following general Taylor polynomial, [3]

$$f(T,P_0) = f(T_0,P_0)\sum_{n=0}^{N} \mathrm{TC}f_n(T_0,P_0)\cdot(T-T_0)^n \qquad (1)$$

where the limit $N \to \infty$ may be used to theoretically include all higher-order terms of T. In Eq. (1), $\mathrm{TC}f(T_0, P_0)$ is the n-th order temperature coefficient of frequency at temperature T_0 and pressure P_0, evaluated as

$$\mathrm{TC}f_n(T_0,P_0) = \left\{\frac{1}{n!\,f(T,P_0)}\frac{\partial^n f(T,P_0)}{\partial T^n}\right\}\Bigg|_{T=T_0} \qquad (2)$$

The device was tested at the wafer level in the Cascade Microtech vacuum probe station, over a wide temperature range from −60 °C to 300 °C, in order to evaluate the

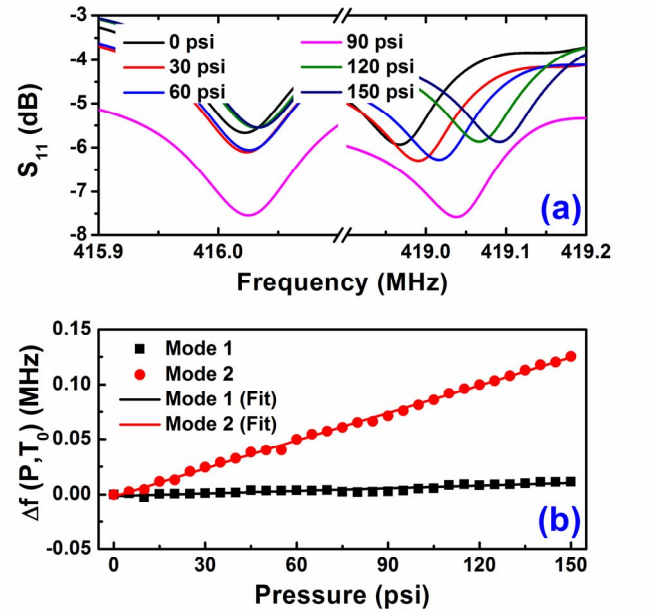

Figure 4: Pressure response of dual-frequency resonating device.
(a) S_{11} response for various pressures applied to the cavity.
(b) Comparison of shifts in the two resonance frequencies of the dual-frequency resonating device.

device's TC*f*. The transmission characteristics were measured using a network analyzer, Agilent E5071B, which is calibrated using the Short-Load-Open-Through (SOLT) method. The S_{11} response of the device at various temperatures is recorded, and the frequency of the resonant mode(s) are extracted.

Fig. 2 presents the fractional variation of resonance frequency for devices without and with OTA. Over the wide temperature range measured, the devices with OTA experience significantly less variation than their reference counterparts without OTA. This points to the effectiveness of OTA as a passive temperature compensation structure.

The S_{11} response of the device with OTA is presented in Fig. 3(a). In each S_{11} curve, the peaks of the resonance frequencies of both modes are evidently shown. Next, these two resonance frequencies were extracted. Fig. 3(b), which illustrates the magnitude of frequency shifts, reveals that these two modes exhibit similar behavior under the effect of ambient temperature. Fig. 3(c) presents that, the extracted TCf_1 at room temperature (20 °C) for both frequencies, using Eq. (2), are 6.25 ppm/°C and 6.66 ppm/°C for modes 1 and 2 respectively. Their turnover temperatures (TOT) are close in value, at 185 °C and 197 °C respectively. A summary of the temperature-dependent parameters of both modes of this dual-frequency device is presented in Table 1.

Pressure Effects

Similar to Eq. (1) and (2) for frequency dependence on temperature, the resonance frequency $f(P,T_0)$ may be described as a function of pressure P at constant temperature T_0, as

Table 1: Summary of TCF characteristics of the reported dual-frequency resonating device.

Res. Freq. #	1	2
TCf_1 (T_{rm}) (ppm/°C)	6.25	6.66
TCf_2 (T_{rm}) (ppb/°C^2)	−9.44	−9.42
Turnover Temp. (°C)	185	197
TCf_2 (TOT) (ppb/°C^2)	−9.43	−9.41

$$f(P,T_0) = f(P_0,T_0)\sum_{n=0}^{N} \mathrm{PC}f_n(P_0,T_0)\cdot(P-P_0)^n \qquad (3)$$

where the limit $N \to \infty$ may be used to theoretically include all higher-order terms of P. In Eq. (1), $\mathrm{PC}f(P_0,T_0)$ is the n-th order temperature coefficient of frequency at pressure P_0 and temperature T_0, evaluated as

$$\mathrm{PC}f_n(P_0,T_0) = \left\{\frac{1}{n!\,f(P,T_0)}\frac{\partial^n f(P,T_0)}{\partial T^n}\right\}\Bigg|_{P=P_0} \qquad (4)$$

Next, an investigation on the ability of this resonator to be used as a pressure sensor was carried out. The resonator chip was assembled on a printed circuit board for readout of microwave parameters. Varying degrees of differential pressure, ranging from 0 to 150 psi (~10 bar), were applied to the backside cavity using a PPCH hydraulic pressure controller. The top of the resonator structure was left in atmospheric pressure. All testing of the device under differential pressure was conducted at the room temperature of 20 °C. The shifts in the S_{11} response over the pressure sweep for both resonance frequencies are presented in Fig. 4(a).

Fig. 4(b) summarizes the shift in resonance frequency over a range of differential pressures applied. Given that the resonance frequency shift of both modes as a function of pressure are highly linear, $N = 1$ was used as the regression model. The second resonance frequency exhibits a PCf_1 of 10.6 times that of the first resonance frequency, due to the presence of differentiated cavity structures.

Fig. 5 highlights the experimental performance of the device as an accurate temperature-compensated pressure sensor. In doing so, the beat frequency was calculated to compensate the reference frequency. [6] In our device, beat frequency f_β is defined as $f_2 - f_1$. The device exhibits its merits in two aspects. Firstly, the output parameter, beat resonance frequency shift, is highly linear, where $R^2 = 0.998$ and non-linearity is 2.28 % Full-Scale (maximum) and 1.20 % F.S. (mean-squared). This implies a high degree of accuracy for this resonating device which is to be used in pressure sensing.

Furthermore, it is observed that the device is highly temperature stable over a wide temperature range (360 °C), thanks to the introduction of OTA as the passive temperature compensation structure. Thermal zero shift (TZS), defined in this case as the change in the beat frequency over the entire temperature range (spanning over 360 °C) at zero differential pressure, is 0.15 % F.S./°C and 55 % of full scale output over 150 psi.

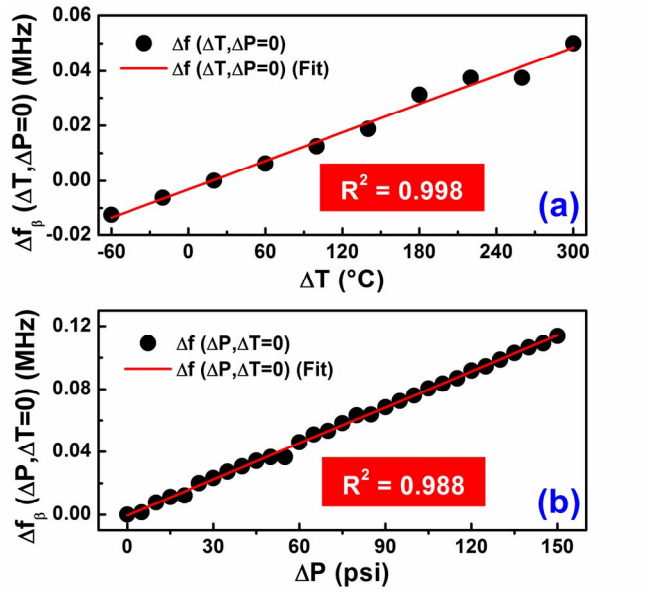

Figure 5: Performance of resonating device for use in pressure sensing, over the measured temperature range. (a) Response of resonating device against varying differential pressure, at constant temperature (20 °C). Sensitivity is 0.67 % full scale (F.S.) / psi; non-linearity is 2.28 % F.S. (best-fit straight line, BFSL) and 1.20 % F.S. (mean-squared NL, BFSL) (b) Response of resonating device against varying temperature, at constant differential pressure (0 psi). Thermal zero shift (TZS) is 0.15 % F.S./°C, or 55 % of full-scale output over 150 psi.

CONCLUSION AND FUTURE WORK

An accurate pressure sensor capable of achieving a non-linearity of 2.28 % F.S. has been experimentally demonstrated. Furthermore, using oxide trench array as a passive temperature compensation structure, the TZS of the device has been reduced over a wide temperature range of 360 °C. This accurate pressure sensor with low temperature effects over a wide temperature range makes it a promising candidate for sensing in ruggedized environments with significant temperature fluctuation.

ACKNOWLEDGMENTS

This work was supported by the Science and Engineering Research Council of Agency for Science, Technology and Research (A*STAR), Singapore, under Grant No. 1421500072.

REFERENCES

[1] X. Mu *et al.*, "Dual mode acoustic wave sensor for precise pressure reading," *Appl. Phys. Lett.*, vol. 105, p. 113607, Sep. 2014.

[2] C.-M. Lin *et al.*, "Thermally compensated aluminum nitride Lamb wave resonators for high temperature applications," *Appl. Phys. Lett.*, vol. 97, 083501, Aug. 2010.

[3] R. Tabrizian, G. Casinovi and F. Ayazi, "Temperature-stable silicon oxide (SilOx) micromechanical resonators," *IEEE Trans. Electron Devices*, vol. 60, no. 8, pp. 2656-2663, Aug. 2013.

[4] P. Kropelnicki *et al.*, "CMOS-compatible ruggedized high-temperature Lamb wave pressure sensor," *J. Micromech. Microeng.*, vol. 23, p. 085018, Jul. 2013.

[5] L. Khine, J. B. W. Soon and J. M. Tsai, "Piezoelectric ALN MEMS resonators with high coupling coefficient," *Proc. 16th Int. Solid-State Sens., Actuators, Microsyst. Conf. (Transducers)*, Beijing, China, Jun. 2011, pp. 526-529.

[6] J. L. Fu, R. Tabrizian and F. Ayazi, "Dual-mode AlN-on-silicon micromechanical resonators for temperature sensing," *IEEE Trans. Electron Devices*, vol. 61, no. 2, pp. 591-597, Feb. 2014.

CONTACT

* C. Sun, tel: +65-67705424; sunc@ime.a-star.edu.sg

A. B. Randles is currently with Invensense Inc., Boston, MA 02110, USA.

P. Singh is currently with Centre for Applied Research in Electronics, Indian Institute of Technology Delhi, New Delhi-110016, India.